Electronic and optical properties of InAs/GaAs nanowire superlattices

Y. M. Niquet[*]

Département de Recherche Fondamentale sur la Matière Condensée, SP2M/L_Sim, CEA Grenoble, 38054 Grenoble Cedex 9, France
(Received 21 June 2006; published 5 October 2006)

The electronic structure of InAs/GaAs nanowire superlattices with radius $R=10$ nm is computed using a semiempirical $sp^3d^5s^*$ tight-binding model, taking strains, piezoelectric fields, and image charge effects into account. The electron-hole interaction is also included in the calculation of the optical properties. Strain relaxation is efficient in nanowire heterostructures, but highly inhomogeneous in thin InAs layers with thickness $t \ll R$. It digs a well in the conduction band that traps the electron at the surface of the nanowire, which might lead to its capture by nearby defects. This well disappears in thicker InAs layers that are almost completely relaxed. The strains and piezoelectric field, however, separate the electron from the hole when increasing t, which strongly reduces the oscillator strength of the exciton.

I. INTRODUCTION

Semiconducting nanowires grown from metal catalysts[1–3] have attracted a lot of interest in the past few years. They provide new insights into the physics of one-dimensional systems, and are promising building blocks for opto- and nanoelectronics.[4] These nanowires are very versatile. In particular, their composition can be modulated along the growth axis,[5,6] which enables the synthesis of high-quality heterostructures with embedded quantum dots or tunnel barriers. InAs/InP,[7,8] GaAs/GaP,[6,9] or InAs/GaAs (Refs. 10 and 11) nanowires, for example, have shown remarkable optical and electrical properties. Nanowire-based devices such as resonant tunneling diodes[12] (RTDs), single-electron transistors,[13] and memories[14] have already been sucessfully realized.

Strain is a fundamental issue in semiconductor heterostructures. It limits the design of conventional, quantum well systems. The coherent epitaxy of thick lattice-mismatched layers has nonetheless been demonstrated in nanowires. Their surface can indeed bend to help relieve the strains. The relaxed strain distribution might, however, be very inhomogeneous. The effects of strains on the electronic properties of the nanowires are, moreover, little known. Previous studies on etched nanowires suggest that the carriers might be localized (in compressed layers) near the surface where strong relaxation takes place.[15–17] This, of course, is not desirable for most experiments and applications.

The electronic properties of (unstrained) GaAs/GaAlAs nanowire superlattices have been computed recently by Persson and Xu.[18] Those of InAs/InP nanowire RTDs had been calculated before[19] without taking inhomogeneous strain relaxation into account. In this work, we compute the structural and electronic properties of InAs/GaAs nanowire superlattices with radius $R=10$ nm, using a semiempirical $sp^3d^5s^*$ tight-binding model. This pair of materials is well suited to a detailed investigation of strain-related issues in semiconductor nanowires. We take the piezoelectric field into account. The effects of the image charges, which arise from the dielectric mismatch between the nanowires and vacuum, and of the electron-hole interaction are also included in the calculation. We show that strain relaxation is indeed efficient in nanowire heterostructures. It is, however, very inhomoge-neous in thin InAs layers with thickness $t \ll R$. Strain relaxation then digs a well in the conduction band that traps the electrons at the surface of the nanowire, which might ease their capture by nearby defects. This well disappears in thicker InAs layers. The strains and piezoelectric field, however, separate the electron from the hole at large t, which reduces the oscillator strength of the exciton.

Section II introduces the models used to compute the structural and electronic properties of the nanowires. The properties of InAs/GaAs nanowire superlattices are then discussed in Sec. III.

II. THEORY

In this section, we first describe the nanowire structures and then the physics included in the tight-binding model: strains, piezoelectric potential, and image charge corrections. We finally discuss the calculation of the exciton.

A. Structures

We consider cylindrical, [111]-oriented InAs/GaAs nanowire superlattices (NWSLs) with the zinc-blende structure. The radius of the nanowires is $R=10$ nm. The thickness of the InAs layers is $4 \leq t \leq 16$ nm. The period of the superlattice, $L \simeq 40$ nm, was chosen large enough to limit elastic coupling between the InAs layers. The dangling bonds at the surface of the nanowires are saturated with hydrogen atoms. The supercell contains $N=569\,600$ atoms.

In the following we let $x=[1\bar{1}0]$, $y=[11\bar{2}]$, and $z=[111]$.

B. Strain relaxation

We assume epitaxial growth. The lattice mismatch of InAs on GaAs is $\varepsilon_\parallel = -6.69\%$. The InAs layers are therefore heavily compressed by the majority material. The surface of the nanowires can, however, bulge to relieve part of the strains. The relaxed atomic positions $\mathbf{R}_i$ are computed using Keating's valence force field[20,21] (VFF) model. The elastic energy depends on the nearest-neighbor (NN) bond lengths and bond angles through bond stretching constants α_{ij} and bond bending constants β_{ijk}:

TABLE I. The VFF parameters d, α, and β for InAs and GaAs. The VFF c_{11}, c_{12}, and c_{44} and internal strain parameter ζ are compared with experimental (Ref. [26]) or *ab initio* (Ref. [27]) data (in parentheses).

Material	d (Å)	α (N/m)	β (N/m)	c_{11} (GPa)	c_{12} (GPa)	c_{44} (GPa)	ζ
InAs	2.623	32.65	7.35	90.27	41.77	39.59	0.63
				(83.29)	(45.26)	(39.59)	(0.64)
GaAs	2.448	39.85	10.86	128.14	51.28	60.40	0.57
				(121.10)	(54.80)	(60.40)	(0.53)

$$E = \sum_{i=1}^{N} \sum_{j}^{\mathrm{NN}} \frac{3\alpha_{ij}}{16 d_{ij}^2} [(\mathbf{R}_j - \mathbf{R}_i)^2 - d_{ij}^2]^2$$
$$+ \sum_{i=1}^{N} \sum_{j,k>j}^{\mathrm{NN}} \frac{3\beta_{ijk}}{16 d_{ij} d_{ik}} \left[(\mathbf{R}_j - \mathbf{R}_i)(\mathbf{R}_k - \mathbf{R}_i) + \frac{d_{ij} d_{ik}}{3} \right]^2. \tag{1}$$

d_{ij} is the equilibrium distance between atoms i and j. In bulk materials, the VFF model only features two elastic constants[22] α and β, which are nonetheless able to reproduce c_{11}, c_{12}, and c_{44} within a few percent. Here we specifically fit α and β onto the bulk modulus $K = (c_{11} + 2c_{12})/3$ and onto c_{44}, in order to reproduce the Poisson ratio ν_{111} along the nanowires:

$$\nu_{111} = 2 \frac{c_{11} + 2c_{12} - 2c_{44}}{c_{11} + 2c_{12} + 4c_{44}}. \tag{2}$$

The parameters of the VFF model are given in Table I. The internal strain parameter, ζ, that describes the relative motion of the two zinc-blende sublattices under uniaxial $\langle 111 \rangle$ strain, also comes out properly. We set $\beta = [\beta_{\mathrm{InAs}} \beta_{\mathrm{GaAs}}]^{1/2}$ on the InAs/GaAs interfaces.[23]

The elastic energy is minimized with respect to the atomic positions and period of the superlattice using a conjugate gradients algorithm.[24] The strain tensor $\hat{\varepsilon}(\mathbf{R}_i)$ is then computed from the atomic positions following the lines of Ref. [25].

C. Piezoelectric potential

Shear strains displace the anions with respect to the cations, which gives rise to a piezoelectric polarization field and potential.[28] This is especially important in $\langle 111 \rangle$-oriented heterostructures. Quantum well superlattices (QWSLs) grown along that direction actually exhibit the largest piezoelectric fields. The first-order polarization density $\mathbf{P}(\mathbf{r})$ reads in the cubic axis set $\{x' = [100], y' = [010], z' = [001]\}$

$$\mathbf{P}(\mathbf{r}) = 2e_{14}(\mathbf{r}) \begin{pmatrix} \varepsilon_{y'z'} \\ \varepsilon_{x'z'} \\ \varepsilon_{x'y'} \end{pmatrix}_{\mathbf{r}}, \tag{3}$$

where e_{14} is the piezoelectric constant ($e_{14} = 0.045$ C/m^2 in InAs and 0.160 C/m^2 in GaAs[26,29]). The piezoelectric potential $V_p(\mathbf{r})$ is the solution of Poisson's equation for the equivalent bound charge density $\rho_p(\mathbf{r}) = -\nabla \mathbf{P}(\mathbf{r})$:

$$\nabla \varepsilon_0 \kappa_0(\mathbf{r}) \nabla V_p(\mathbf{r}) = -\rho_p(\mathbf{r}), \tag{4}$$

ε_0 being the vacuum permittivity and $\kappa_0(\mathbf{r})$ the static dielectric constant.

As an example (and for later comparison with NWSLs), the piezoelectric field in a $[111]$-oriented QWSL is derived in Appendix A. In NWSLs, the piezoelectric polarization density is calculated from the strains on each cation using Eq. (3). The bound charge density $\rho_p(\mathbf{r}) = -\nabla \mathbf{P}(\mathbf{r})$ and the piezoelectric potential $V_p(\mathbf{r})$ [Eq. (4)] are then computed with a finite-difference method. We set $\kappa_0 = 15$ inside the nanowires and $\kappa_0 = 1$ (vacuum) outside. Details can be found in Appendix B.

D. Image charge corrections

An additional electron traveling in a solid repels nearby valence electrons, thus dragging a so-called Coulomb hole around.[30] The work needed to form this Coulomb hole makes a significant contribution to the band-gap energy of semiconductors. In bulk materials, the charge cast out from the Coulomb hole goes to "infinity." In NWSLs, however, this charge is repelled at the surface of the nanowires.[31,32] The interaction between the additional electron and these (negative) surface image charges decreases the affinity and raises the conduction band states. Conversely, the hole added upon ionization of the NWSL gets surrounded by a cloud of valence electrons, leaving positive image charges at the surface. The repulsion between the hole and its image charges also increases the ionization energy and lowers the valence band states. The image charges (also known as self-energy) corrections therefore result in a substantial opening of the one-particle band gap of the nanowires.

We have discussed the underlying physics and theory in Ref. [33]. In a semiclassical approach,[34] the effect of the image charges can be modeled by a local potential $\pm\Sigma(\mathbf{r})$ (+ for the electrons, − for the holes), where

$$\Sigma(\mathbf{r}) = \frac{e^2}{2} \lim_{\mathbf{r}' \to \mathbf{r}} \left(V(\mathbf{r}, \mathbf{r}') - \frac{1}{\varepsilon_0 \kappa_\infty(\mathbf{r}) |\mathbf{r} - \mathbf{r}'|} \right). \tag{5}$$

$V(\mathbf{r}, \mathbf{r}')$ is the potential created at $\mathbf{r}'$ by a particle with unit charge located at $\mathbf{r}$, computed using the high-frequency dielectric constant[35] $\kappa_\infty = 12$. $\Sigma(\mathbf{r})$ is actually half the potential created at $\mathbf{r}$ by the image charges following the particle. It is plotted in Fig. 1 for a nanowire with radius $R = 10$ nm. $\Sigma(\mathbf{r})$ is positive inside the nanowire and increases as the particle approaches the surface, thus enhancing lateral confinement.
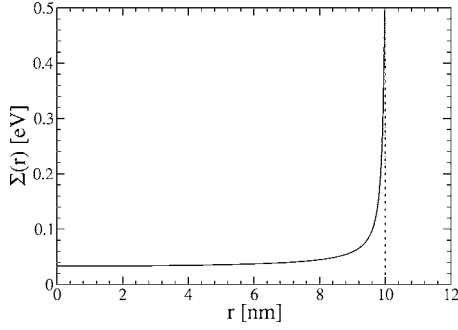
FIG. 1. The image charge potential $\Sigma(r)$ in a nanowire with radius $R=10$ nm.

E. Tight-binding calculations

The one-particle states of the NWSLs are computed with a first-nearest-neighbor, two-center orthogonal $sp^3d^5s^*$ tight-binding (TB) model.[36,37] Our approach is based on Jancu *et al.*'s parametrization taking strains and spin-orbit coupling into account.[38] Jancu *et al.* initially introduced an on-site, strain-dependent term in their model that lifts the degeneracy of the d orbitals under uniaxial $\langle 001 \rangle$ strain. They reproduced in that way the valence band deformation potential b. Their model does not, however, reproduce the shear deformation potential d (the splitting between the heavy- and light-hole bands under uniaxial $\langle 111 \rangle$ strain). Boykin *et al.*'s parametrization,[39] which also includes strain-dependent diagonal energy shifts, does not perform much better ($d=-4.8$ eV in InAs). Indeed, on-site, off-diagonal couplings between the p and/or d orbitals are needed to reproduce the valence band splittings under *arbitrary* strains. We therefore generalized Jancu *et al.*'s description by adding a strain-dependent coupling matrix between the p and between the d orbitals. The details of this model will be published elsewhere.[40] The TB valence band deformation potentials b and d are compared to Van de Walle's *ab initio* data[41] in Table II.

The conduction and valence band hydrostatic deformation potentials a_c and a_v, as well as the unstrained valence band offset Δ_{VB} between InAs and GaAs, are other key inputs for the TB parametrization. Their values are still, unfortunately, controversial.[41–43] We again chose[40] to reproduce the *ab initio* data of Van de Walle[41] (see Table II). We set $\Delta_{VB}=0.2$ eV.

TABLE II. The TB and experimental (Ref. 26) (Expt.) band gap or *ab initio* (Ref. 41) deformation potentials of InAs and GaAs, in eV.

	InAs		GaAs	
	TB	Expt.	TB	Expt.
E_g	0.42	0.42	1.52	1.52
a_c	−5.12	−5.08	−7.60	−7.17
a_v	1.00	1.00	1.16	1.16
b	−1.55	−1.55	−1.90	−1.90
d	−3.10	−3.10	−4.23	−4.23

The piezoelectric potential and image charge effects[44] are included in the Hamiltonian. We look for a few eigenpairs around the band gap using a Jacobi-Davidson algorithm[45,46] as discussed in Ref. 33.

F. Excitonic corrections

The electron and hole in bulk InAs are weakly coupled because the former is light (effective mass $m^*=0.023m_0$) and because Coulomb screening is effective ($\kappa_\infty=12$). The binding energy of the bulk exciton is only $E_X \sim 1$ meV and its radius $a_X \sim 35$ nm is much larger than the dimensions of the InAs layers considered in this work. In this strong-confinement regime, the exciton can be approximated as an uncorrelated electron-hole pair with wave function

$$\psi(\mathbf{r}_e, \mathbf{r}_h) = \psi_e(\mathbf{r}_e)\psi_h(\mathbf{r}_h), \tag{6}$$

$\mathbf{r}_e$ and $\mathbf{r}_h$ being the positions of the electron and hole. We optimize the electron wave function ψ_e in the electrostatic potential $V_h(\mathbf{r})$ created by the hole, and the hole wave function ψ_h in the electrostatic potential $V_e(\mathbf{r})$ created by the electron. The self-consistent equations read for the electron

$$\hat{H}_0|\psi_e\rangle - e\hat{V}_h|\psi_e\rangle = \varepsilon_e|\psi_e\rangle, \tag{7}$$

where[47]

$$\boldsymbol{\nabla}\varepsilon_0\kappa_\infty(\mathbf{r})\,\boldsymbol{\nabla}\,V_h(\mathbf{r}) = -e|\psi_h(\mathbf{r})|^2. \tag{8}$$

$\hat{H}_0$ is the one-particle tight-binding Hamiltonian, including the strains, piezoelectric potential, and image charge effects. The self-consistent equations are similar for the hole. $V_e(\mathbf{r})$ and $V_h(\mathbf{r})$ are again computed with a finite-difference method (see Appendix B). The exciton energy finally reads $E_0 = \langle\psi_e|\hat{H}_0|\psi_e\rangle - \langle\psi_h|\hat{H}_0|\psi_h\rangle - W$, where $W=e\langle\psi_e|\hat{V}_h|\psi_e\rangle = -e\langle\psi_h|\hat{V}_e|\psi_h\rangle$ is the Coulomb interaction energy between the two particles.

III. RESULTS

In this section, we first discuss the strain distribution, then the piezoelectric potential in the NWSLs; we last analyze their electronic and optical properties.

A. Strain relaxation

The hydrostatic strain $\delta\Omega/\Omega = \varepsilon_{xx}+\varepsilon_{yy}+\varepsilon_{zz}$ in 4- and 16-nm-thick InAs layers is plotted in Fig. 2. $\delta\Omega/\Omega$ is the (first-order) variation of the volume of the unit cell with reference to the unstrained material. In an InAs/GaAs QWSL grown on GaAs, the strains in the InAs layers would be $\varepsilon_{xx}=\varepsilon_{yy}=-6.69\%$ and $\varepsilon_{zz}=-\nu_{111}\varepsilon_{xx}=3.81\%$, resulting in a large, uniform compression $\delta\Omega/\Omega=-9.56\%$. In small enough NWSLs, the InAs layers can relax part of these strains by protruding outward. This is clearly evidenced in Fig. 2. Strain relaxation first takes place at the surface of the nanowire, then extends deeper and deeper inside with increasing t. The periphery of the InAs layers is even overrelaxed ($\delta\Omega/\Omega > 0$) to help relieve strains in the core. The expansion of the InAs layers goes with a buildup of tensile strains in
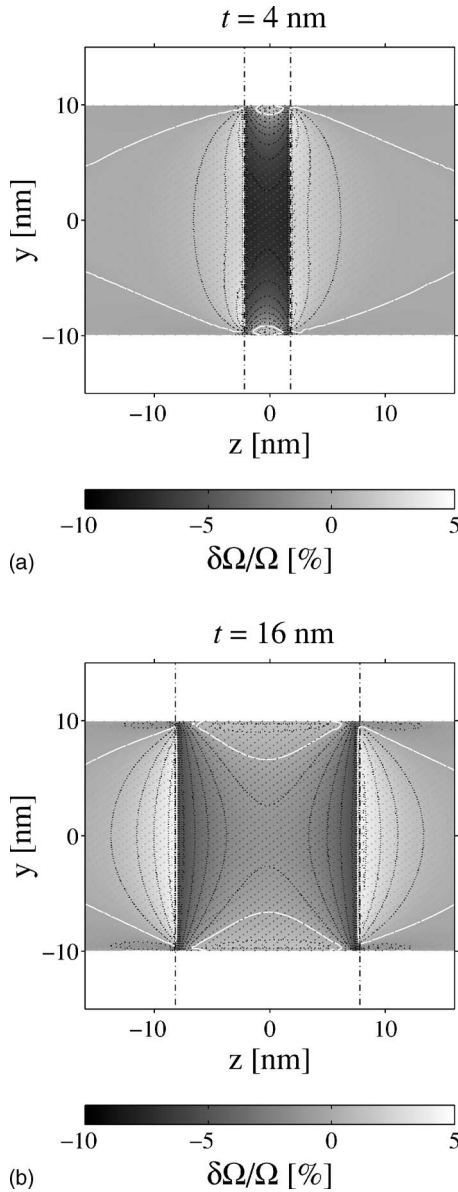
(a)

(b)

FIG. 2. The hydrostatic strain $\delta\Omega/\Omega$ in 4- and 16-nm-thick InAs layers. The dots are the In/Ga atoms in the (yz) plane of the plot. The vertical, dash-dotted lines delimit the InAs layers. The spacing between isolevel curves is 1%, the white one being $\delta\Omega/\Omega=0$.

GaAs that slowly relax away from the interfaces. As shown in Fig. 3, the competition between strain relaxation in InAs and GaAs gives rise to large shear strains at the interfaces, InAs pushing outward on one side and GaAs pulling inward on the other.

The hydostatic strain at the center of the InAs layers decreases from $\delta\Omega/\Omega=-7.24\%$ for $t=4$ nm to $\delta\Omega/\Omega=-1.17\%$ for $t=16$ nm. Alternatively, the residual strain in the InAs layers can be characterized by the total variation $\Delta V/V$ of their volume with reference to the free-standing case (the average $\delta\Omega/\Omega$). $\Delta V/V$ is plotted in Fig. 4. It is already half the full strain (-9.56%) for $t=4$ nm, and drops below -1% for $t=16$ nm, showing that the InAs layers are almost completely relaxed. $\Delta V/V$ can be expected to depend on t/R for small[17] enough t (but on $1/t$ for large[48] t). This indeed seems
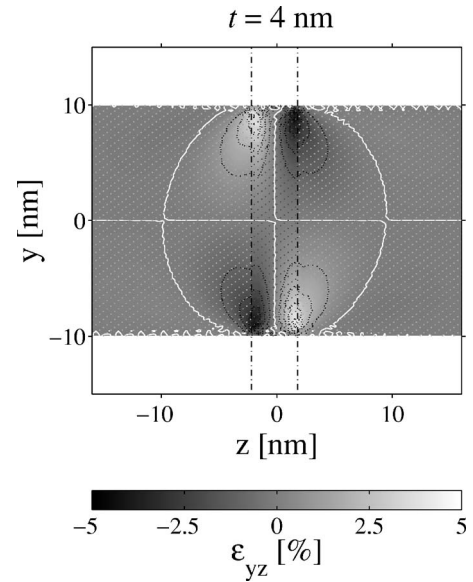

FIG. 3. The shear strain ε_{yz} in a 4-nm-thick InAs layer. The spacing between isolevel curves is 1%, the white one being $\varepsilon_{yz}=0$.

to be the case in Fig. 4, which gathers data for $R=16$ and 20 nm.

We would finally like to stress that these calculations, although showing strong elastic relaxation, cannot rule out the formation of dislocations or the Stranski-Krastanov-like growth of InAs pyramids in the nanowires.

B. Piezoelectric potential

The piezoelectric potential in 4- and 16-nm-thick InAs layers is plotted in Fig. 5. In an InAs/GaAs QWSL, the piezoelectric polarization density would be $\mathbf{P}=(2e_{14}/\sqrt{3}) \times(\varepsilon_{zz}-\varepsilon_{\parallel})\mathbf{z}$ in InAs (and zero in GaAs). $\mathbf{P}$ would transfer bound charge from one interface to the other, making each layer look like a parallel plate capacitor (see Appendix A). The piezoelectric field $\mathbf{E}=E_z\mathbf{z}$ would thus be uniform in InAs. NWSLs still behave (in a first approximation) as finite parallel plate capacitors, $\rho_p(\mathbf{r})$ being peaked around the interfaces. The interpretation of $\rho_p(\mathbf{r})$ might, however, be different. There is, in particular, an additional transfer of
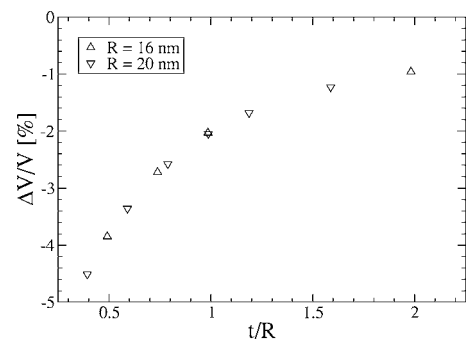

FIG. 4. The variation $\Delta V/V$ of the volume of the InAs layers with reference to the free-standing case, as a function of t/R. Data for $R=16$ and 20 nm are represented.
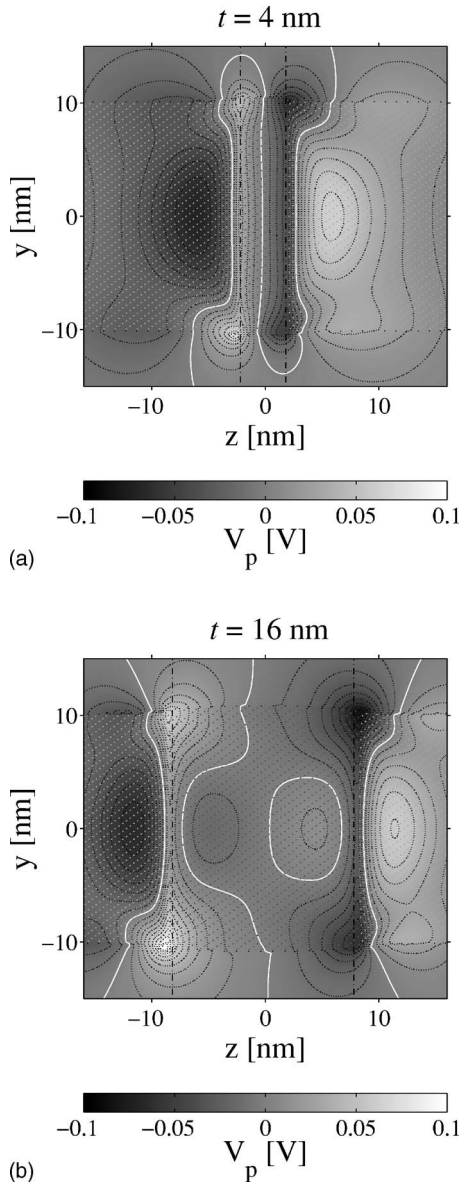
(a)

(b)

FIG. 5. The piezoelectric potential $V_p(\mathbf{r})$ in 4- and 16-nm-thick InAs layers. The spacing between isolevel curves is 10 mV, the white one being $V_p(\mathbf{r})=0$.

charges from strained GaAs to the interfaces. This enhances the piezoelectric field in the barriers, but has little effect in the InAs layers.

The piezoelectric field is almost uniform in InAs when $t \ll R$. E_z is about 1.5×10^7 V/m at the center of the 4-nm-thick layer. This is 2.5 times smaller than in the equivalent QWSL ($E_z=3.7 \times 10^7$ V/m) due to strain relaxation. The piezoelectric field is much more inhomogeneous at larger t. Thick InAs layers are indeed almost completely relaxed. The polarization density **P** is therefore sizable only near the interfaces. $\rho_p(\mathbf{r})$ becomes more diffuse, with tails of charge inside InAs. These tails screen the interfaces and even reverse the piezoelectric field in some parts of the layer, as evidenced by the shape of the $V_p(\mathbf{r})=0$ line in Fig. 5. We will discuss the effect of the piezoelectric field on the electronic structure in Sec. III D.
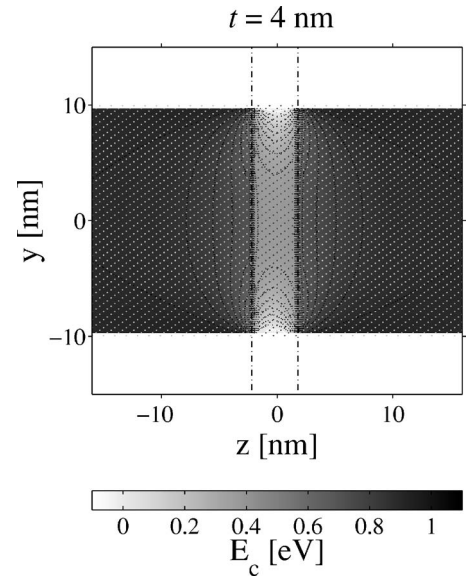

FIG. 6. The conduction band profile $E_c(\mathbf{r})$ in a 4-nm-thick InAs layer. The energy is measured with respect to the conduction band edge of bulk, unstrained InAs. The spacing between isolevel curves is 50 mV, the white one being $E_c(\mathbf{r})=0$.

C. Confinement potentials

Strain relaxation is very inhomogeneous in the thinnest InAs layers. It mostly takes place in a shell of width $\sim t$ at the surface of the nanowire, leaving the core heavily compressed. This might have a significant impact on their electronic properties. Compressive (tensile) strains indeed shift the conduction band upward (downward). The first-order shift is proportional to the hydrostatic strain:

$$\Delta E_c = a_c \frac{\delta \Omega}{\Omega}. \qquad (9)$$

The strain distributions of Fig. 2 should therefore dig a well in the conduction band at the surface of the nanowires.

The conduction band profile $E_c(\mathbf{r})$ in a 4-nm-thick InAs layer is plotted in Fig. 6, including chemical confinement and strains. The energy is measured with respect to the conduction band edge of bulk, unstrained InAs. For consistency, $E_c(\mathbf{r})$ was computed as the TB conduction band energy in a bulk material with the same strains as in the nanowire. This takes nonlinear effects beyond Eq. (9) into account. The conduction band is shifted upward by about 380 meV at the center of the InAs layer. Strain relaxation, however, digs (as expected) a $\simeq 400$ meV deep well at the surface of the nanowire. This well becomes more and more shallow with increasing t, as strain relaxation gains the whole layer. It is only $\simeq 140$ meV deep for $t=16$ nm. We will discuss its effect on the electronic structure of the nanowires in Sec. III D.

The dependence of the valence band edge energies on strains is much more intricate.[49] The heavy-hole potential, which controls the confinement of the lowest-lying states, is much flatter across the nanowire than $E_c(\mathbf{r})$. However, in thick InAs layers, the residual compressive strain near the interfaces digs a shallow well for the holes that might help
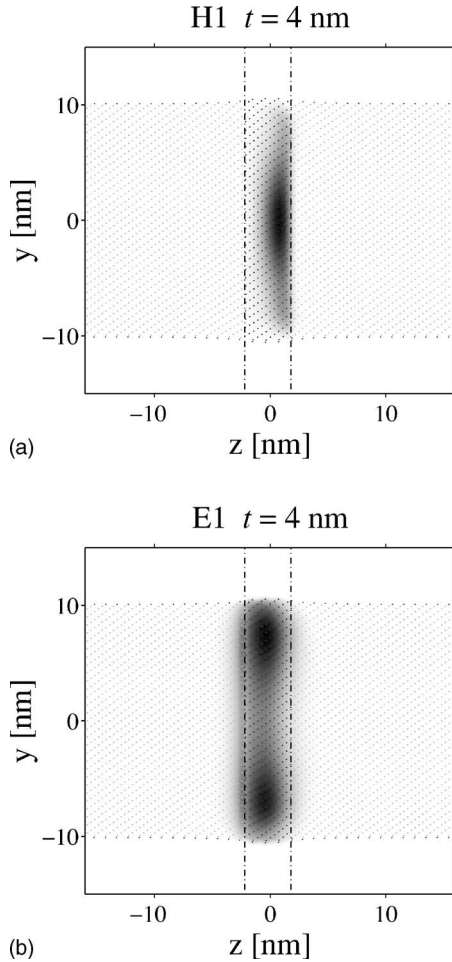
FIG. 7. The square of the highest hole (H1) and lowest electron (E1) wave functions in a 4-nm-thick InAs layer. Their energies (with respect to the valence band edge of bulk InAs) are $E(H1)=$ -0.011 eV and $E(E1)=0.946$ eV.

FIG. 8. The square of the highest hole (H1) and lowest electron (E1) wave functions in a 16-nm-thick InAs layer. Their energies are $E(H1)=-0.007$ eV and $E(E1)=0.593$ eV.

localization there. Strains typically shift the heavy-hole energies $\simeq 65$ meV upward at the center of the 4-nm-thick InAs layer.

D. Electronic structure

The lowest-lying electron (E1) and hole (H1) wave functions in a 4-nm-thick InAs layer are plotted in Fig. 7 (not including the excitonic correction). Their energies (with respect to the valence band edge of bulk InAs) are $E(E1)$ $=0.946$ eV and $E(H1)=-0.011$ eV. As discussed in the previous section, strain relaxation digs a well in the conduction band at the surface of the nanowire. This well, though partially filled by the image charge potential (Fig. 1), traps the electron. The hole remains, on the contrary, peaked along the nanowire axis. It is, however, pushed against the rightmost interface by the piezoelectric field (Fig. 5). The H1 wave function has a clear "heavy-hole" character, as expected for quantum-well-like systems under compressive strains.[50]

Trapping the electron so close to the surface is not very desirable for most experiments and applications. Nearby surface defects might indeed capture the electron more easily.
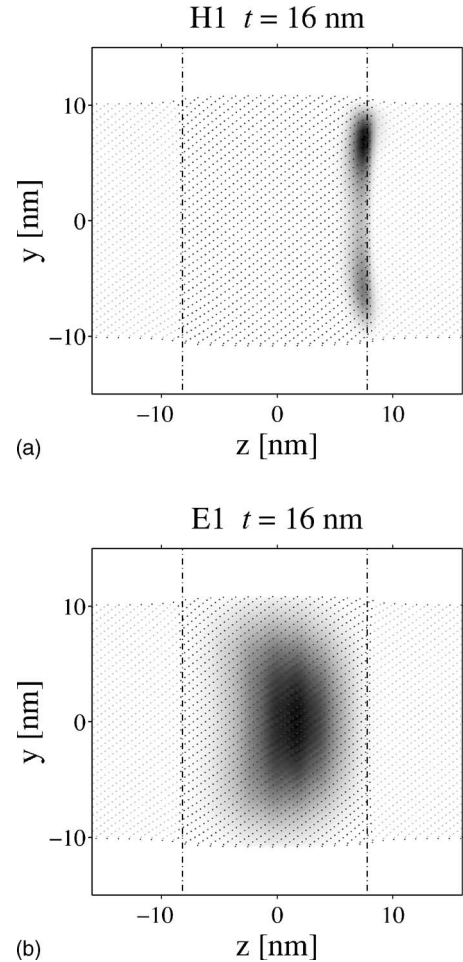
These consequences of inhomogeneous strain relaxation have been evidenced before in etched nanowires.[15–17] Yet the well in the conduction band becomes shallow at larger t, as discussed in Sec. III C. The opening in the center of the E1 wave function actually closes with increasing t and is not apparent any more beyond $t=8$ nm. This is clearly illustrated in Fig. 8, for a 16-nm-thick InAs layer. The strains and piezoelectric field, however, still squeeze the H1 wave function against the rightmost interface. The hole is actually trapped in hollows[51] of the piezoelectric potential located near the surface of the nanowire (see Fig. 5). The strains and piezoelectric field thus separate the electron from the hole, which might degrade the optical properties of the nanowire.

Table III illustrates the main trends as a function of t. The E1 energy drops from $E(E1)=0.946$ eV for t $=4$ nm to $E(E1)=0.593$ eV for $t=16$ nm. The quantum confinement and average conduction band energy in InAs [see Eq. (9) and Fig. 4] indeed rapidly decrease with increasing t. The hole energy, on the other hand, is almost constant. The effects of strains, quantum confinement, and piezoelectricity actually cancel each other on the valence band side. The electron, which is heavier than the hole, is not as sensitive to the piezoelectric field, the expectation value of $V_p(\mathbf{r})$ being much larger for H1 than for E1.

TABLE III. Energy (E), strain-induced shift (Δ_s), expectation value of the piezoelectric potential ($\langle V_p \rangle$), and image charge correction ($\pm\langle\Sigma\rangle$) as a function of the thickness t of the InAs layers, for the lowest-lying hole (H1) and electron (E1) states.

t (nm)		E (eV)	Δ_s (meV)	$\langle V_p \rangle$ (meV)	$\pm\langle\Sigma\rangle$ (meV)
4.0	H1	−0.011	48.7	14.5	−41.5
	E1	0.946	140.5	−1.1	50.0
8.0	H1	−0.010	48.5	33.4	−46.8
	E1	0.741	98.8	2.3	47.8
16.0	H1	−0.007	37.1	31.6	−42.5
	E1	0.593	35.9	2.6	42.7

Taking the electron-hole interaction into account does not change the whole picture. The screening is indeed efficient inside the nanowires, the electron and hole potentials $V_e(\mathbf{r})$ and $V_h(\mathbf{r})$ being quite smooth in the InAs layers. The exciton energy is plotted in Fig. 9. It decreases (following the E1 energy) from $E_0 = 0.870$ eV for $t = 4$ nm down to $E_0 = 0.523$ eV for $t = 16$ nm. The electron-hole interaction energy W, plotted in the inset of Fig. 9, is much larger than in the bulk, and weakly dependent on t. It is actually enhanced by the interaction of the electron with the (positive) image charges of the hole, and by the interaction of the hole with the (negative) image charges of the electron. We may therefore expect large cancellations between the self-energy (interaction of each particle with its own image charges) and the excitonic corrections, the exciton as a whole being a neutral excitation. This is supported by the data in Table III. As a matter of fact, the overall effect of the Coulomb interactions (self-consistent self-energy + excitonic corrections) is a net increase of the H1→E1 transition energy by ≲15 meV.

The oscillator strength[52] for light polarized along x,

$$F_x = \frac{2}{m_0} \frac{|\langle \psi_e | p_x | \psi_h \rangle|^2}{E_0}, \qquad (10)$$

is finally plotted in Fig. 10 (m_0 is the free-electron mass and $p_x = -i\hbar \partial/\partial x$). It was computed following the lines of Ref.
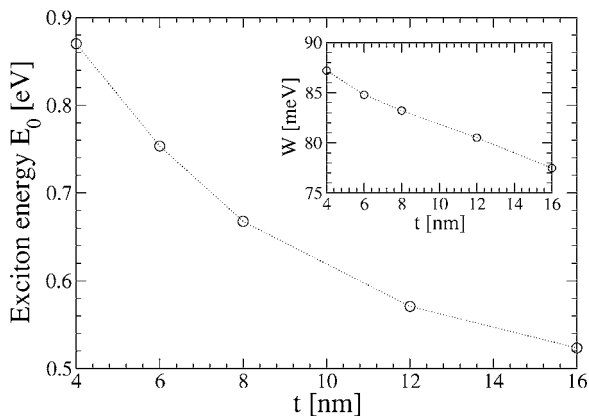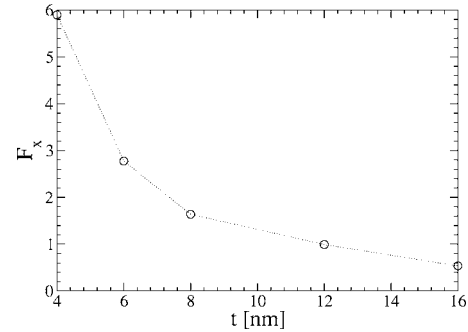

FIG. 10. The oscillator strength F_x as a function of the thickness t of the InAs layers.

53. As expected, F_x decreases monotonically with increasing t, due to the separation of the electron and the hole by the piezoelectric field. The results are similar for F_y, while $F_z \simeq 0$. It might therefore be, unfortunately, quite difficult to observe light emisson from thick InAs layers at low temperatures.

IV. CONCLUSION

We have computed the electronic structure of strained InAs/GaAs nanowire superlattices using a semiempirical $sp^3d^5s^*$ tight-binding model. We have shown that strain relaxation, although efficient, can dig a well in the conduction band of the thinnest InAs layers, which traps the electrons at the surface of the nanowire. This is not desirable for most applications. This well, however, disappears when the thickness of the InAs layers is comparable with the radius of the nanowire. The strains and piezoelectric potential, however, separate the electron from the hole in that limit, which degrades the optical properties of the superlattice. Similar trends can be expected in other heterostructures such as InAs/InP nanowires, though in a different range of dimensions (the lattice mismatch being twice smaller). We stress that strain relaxation would raise an additional barrier (instead of a well) at the surface of layers under tensile strain. The growth of a shell around the nanowires might also homogenize the strain distribution and prevent the formation of such a surface well.

APPENDIX A: PIEZOELECTRIC FIELD IN A [111]-ORIENTED QUANTUM WELL SUPERLATTICE

In a (hypothetical) InAs/GaAs QWSL grown on GaAs, the in-plane and longitudinal strains in the InAs layers would be $\varepsilon_\parallel = -6.69\%$ and $\varepsilon_\perp = \nu_{111}\varepsilon_\parallel = 3.81\%$. In the cubic axis set, the

FIG. 9. The exciton energy E_0 and Coulomb interaction energy W (inset) as a function of the thickness t of the InAs layers.

shear strains would thus be $\varepsilon_{x'y'}=\varepsilon_{y'z'}=\varepsilon_{x'z'}=(\varepsilon_\perp-\varepsilon_\parallel)/3$. The polarization density in the InAs layers would therefore be aligned with the growth axis:

$$P_z = \frac{2}{\sqrt{3}} e_{14}(\varepsilon_\perp - \varepsilon_\parallel). \tag{A1}$$

$\rho_p(\mathbf{r})$ hence reduces to two sheets of charges with uniform density $\sigma=-P_z$ on one interface and $\sigma=+P_z$ on the other. The electric field in the InAs layers then reads

$$E_z = \frac{2}{\varepsilon_0 \kappa_0 \sqrt{3}} \frac{L-t}{L} e_{14}(\varepsilon_\perp - \varepsilon_\parallel). \tag{A2}$$

For example, the electric field in a 4 nm InAs/36 nm GaAs QWSL would be $E_z=3.7\times10^7$ V/m (assuming a uniform dielectric constant $\kappa_0=15$).

APPENDIX B: COMPUTATIONAL DETAILS

Poisson's equation [Eq. (4)] is solved with a finite-difference (FD) method[54] on a nonuniform, tensor product three-dimensional grid. We use different grids and boundary conditions for the piezoelectric potential and exciton problems. $V_p(\mathbf{r})$ is computed at $\approx 15\times10^6$ points in a $87.5\times87.5\times40$ nm^3 box. Periodic boundary conditions are applied in the z direction, while Dirichlet $[V_p(\mathbf{r})=0]$ boundary conditions are applied in the x and y directions. The piezoelectric potential indeed decreases very rapidly outside the nanowire given its dipolar nature. The spacing between grid lines is as small as 2 Å in the InAs layers. $V_e(\mathbf{r})$ and $V_h(\mathbf{r})$ are computed at $\approx 16\times10^6$ points in a 140×140

$\times140$ nm^3 box. This box contains many superperiods, the central one only being charged with an electron or a hole. We use the potential created by a point charge located at the center of the nanowire, computed with Fourier-Bessel series,[55] as boundary conditions. The linear system of equations that follows from the discretization of Poisson's equation is solved with a conjugate-gradient method preconditioned with a diagonal incomplete LU decomposition.[56]

The charges and potentials are transferred between the atoms and FD grid using finite support approximations for the square of the atomic orbitals $|\psi|^2(\mathbf{r}-\mathbf{R}_i)$:

$$|\psi|^2(\mathbf{r} - \mathbf{R}_i) = f(x-x_i)f(y-y_i)f(z-z_i), \tag{B1}$$

where

$$f(t) = \begin{cases} \dfrac{15}{16\Delta}\left[1 - \left(\dfrac{t}{\Delta}\right)^2\right]^2 & \text{if } |t| < \Delta, \\ 0 & \text{otherwise.} \end{cases} \tag{B2}$$

We choose $\Delta=2.54$ Å for semiconductor atoms and $\Delta=1.90$ Å for hydrogen atoms, although this has little influence on the final result. The overlaps between the atomic orbitals and the FD mesh are easily obtained from Eqs. (B1) and (B2). To compute the piezoelectric potential, we first define the total piezoelectric polarization $\bar{\mathbf{P}}_i=\Omega_i\mathbf{P}(\mathbf{R}_i)$ for each cation, where $\Omega_i=16d^3[1+\text{Tr}\,\hat{\varepsilon}(\mathbf{R}_i)]/(3\sqrt{3})$ is the average volume occupied by atom i. $\bar{\mathbf{P}}_i$ is likewise transferred to the FD grid before computing the piezoelectric bound charge density $\rho_p(\mathbf{r})=-\boldsymbol{\nabla}\mathbf{P}(\mathbf{r})$ and solving Poisson's equation for $V_p(\mathbf{r})$.

---

*Electronic address: yniquet@cea.fr

[1] A. M. Morales and C. M. Lieber, Science **279**, 208 (1998).

[2] A. I. Persson, M. W. Larsson, S. Stenström, B. J. Ohlsson, L. Samuelson, and L. R. Wallenberg, Nat. Mater. **3**, 677 (2004).

[3] K. A. Dick, K. Deppert, T. Mårtensson, B. Mandl, L. Samuelson, and W. Seifert, Nano Lett. **5**, 761 (2005).

[4] Y. Xia, P. Yang, Y. Sun, Y. Wu, B. Mayers, B. Gates, Y. Yin, F. Kim, and H. Yan, Adv. Mater. (Weinheim, Ger.) **15**, 353 (2003).

[5] Y. Wu, R. Fan, and P. Yang, Nano Lett. **2**, 83 (2002).

[6] M. S. Gudiksen, L. J. Lauhon, J. Wang, D. C. Smith, and C. M. Lieber, Nature (London) **415**, 617 (2002).

[7] M. T. Björk, B. J. Ohlsson, T. Sass, A. I. Persson, C. Thelander, M. H. Magnusson, K. Deppert, L. R. Wallenberg, and L. Samuelson, Appl. Phys. Lett. **80**, 1058 (2002).

[8] M. T. Björk, B. J. Ohlsson, T. Sass, A. I. Persson, C. Thelander, M. H. Magnusson, K. Deppert, L. R. Wallenberg, and L. Samuelson, Nano Lett. **2**, 87 (2002).

[9] C. P. T. Svensson, W. Seifert, M. W. Larsson, L. R. Wallenberg, J. Stangl, G. Bauer, and L. Samuelson, Nanotechnology **16**, 936 (2005).

[10] B. J. Ohlsson, M. T. Björk, A. I. Persson, C. Thelander, L. R. Wallenberg, M. H. Magnusson, K. Deppert, and L. Samuelson, Physica E (Amsterdam) **13**, 1126 (2002).

[11] N. Panev, A. I. Persson, N. Sköld, and L. Samuelson, Appl. Phys.

Lett. **83**, 2238 (2003).

[12] M. T. Björk, B. J. Ohlsson, C. Thelander, A. I. Persson, K. Deppert, L. R. Wallenberg, and L. Samuelson, Appl. Phys. Lett. **81**, 4458 (2002).

[13] C. Thelander, T. Martenson, M. T. Björk, B. J. Ohlsson, M. W. Larsson, L. R. Wallenberg, and L. Samuelson, Appl. Phys. Lett. **83**, 2052 (2003).

[14] C. Thelander, H. A. Nilsson, L. E. Jensen, and L. Samuelson, Nano Lett. **5**, 635 (2005).

[15] H. Straub, G. Brunthaler, W. Faschinger, G. Bauer, and C. Vieu, J. Cryst. Growth **159**, 451 (1996).

[16] Y. M. Niquet, C. Priester, and H. Mariette, Phys. Rev. B **55**, R7387 (1997).

[17] Y. M. Niquet, C. Priester, C. Gourgon, and H. Mariette, Phys. Rev. B **57**, 14850 (1998).

[18] M. P. Persson and H. Q. Xu, Phys. Rev. B **73**, 035328 (2006).

[19] M. Zervos and L. F. Feiner, J. Appl. Phys. **95**, 281 (2004).

[20] P. N. Keating, Phys. Rev. **145**, 637 (1966).

[21] R. M. Martin, Phys. Rev. B **1**, 4005 (1970).

[22] We set as usual $\beta_{\text{In-As-In}}=\beta_{\text{As-In-As}}=\beta_{\text{InAs}}$ and $\beta_{\text{Ga-As-Ga}}=\beta_{\text{As-Ga-As}}=\beta_{\text{GaAs}}$.

[23] The elastic constants of bonds involving a hydrogen atom are rescaled to those of the underlying material; e.g., $\alpha_{\text{In-H}}=\alpha_{\text{InAs}}d_{\text{InH}}/d_{\text{InAs}}$ and $\beta_{\text{In-As-H}}=\beta_{\text{InAs}}d_{\text{InH}}/d_{\text{InAs}}$.

[24] W. H. Press, S. A. Teukolsky, W. T. Vetterling, and B. P. Flannery, *Numerical Recipes in Fortran* (Cambridge University Press, Cambridge, U.K., 1992).

[25] C. Pryor, J. Kim, L. W. Wang, A. J. Williamson, and A. Zunger, J. Appl. Phys. **83**, 2548 (1998).

[26] *Physics of Group IV Elements and III–V Compounds*, edited by O. Madelung, M. Schulz, and H. Weiss, Landolt-Börnstein, New Series, Group III, Vol. 17, Pt. A (Springer-Verlag, New York, 1982).

[27] S. de Gironcoli, S. Baroni, and R. Resta, Phys. Rev. Lett. **62**, 2853 (1989).

[28] D. L. Smith and C. Mailhiot, Rev. Mod. Phys. **62**, 173 (1990).

[29] The piezoelectric constants are actually negative when a cation is placed at the origin and an anion is placed at $a(111)/4$ (as in our calculation); see G. Arlt and P. Quadflieg, Phys. Status Solidi **25**, 323 (1968).

[30] J. C. Inkson, *Many-Body Theory of Solids* (Plenum, New York, 1984).

[31] C. Delerue and M. Lannoo, *Nanostructures: Theory and Modelling* (Springer, New York, 2004).

[32] C. Delerue, G. Allan, and M. Lannoo, Phys. Rev. Lett. **90**, 076803 (2003).

[33] Y. M. Niquet, A. Lherbier, N. H. Quang, M. V. Fernández-Serra, X. Blase, and C. Delerue, Phys. Rev. B **73**, 165319 (2006).

[34] This semiclassical approach follows from suitable approximations to the *GW* method; see L. Hedin and S. Lundqvist, Solid State Phys. **23**, 1 (1969).

[35] We assume that the ions are too slow to follow the particle and contribute to the image charge corrections, and thus use κ_∞ instead of κ_0 in Eq. (5). Since the electrons and holes are localized in the InAs layers, the ions might still respond to the *average* electron and hole distribution (also see Ref. 47). Likewise, we neglect any difference between the κ_∞'s of InAs and GaAs.

[36] J. C. Slater and G. F. Koster, Phys. Rev. **94**, 1498 (1954).

[37] A. Di Carlo, Semicond. Sci. Technol. **18**, R1 (2003).

[38] J.-M. Jancu, R. Scholz, F. Beltram, and F. Bassani, Phys. Rev. B **57**, 6493 (1998).

[39] T. B. Boykin, G. Klimeck, R. C. Bowen, and F. Oyafuso, Phys. Rev. B **66**, 125207 (2002).

[40] Y. M. Niquet (unpublished).

[41] C. G. Van de Walle, Phys. Rev. B **39**, 1871 (1989).

[42] Su-Huai Wei and A. Zunger, Phys. Rev. B **60**, 5404 (1999).

[43] Y.-H. Li, X. G. Gong, and Su-Huai Wei, Appl. Phys. Lett. **88**, 042104 (2006).

[44] The electron and hole states are not orthogonal anymore since $\Sigma(\mathbf{r})$ enters into the Hamiltonian with a different sign for each kind of quasiparticle. This would, however, be the outcome of any more elaborate quasiparticle theory such as the *GW* method (Ref. 34). The actual overlap between the electron and hole wave functions is at most 2.5×10^{-5}.

[45] G. L. G. Sleijpen and H. A. Van der Vorst, SIAM J. Matrix Anal. Appl. **17**, 401 (1996); SIAM Rev. **42**, 267 (2000).

[46] G. Sleijpen and H. Van der Vorst, in *Templates for the Solution of Algebraic Eigenvalue Problems: A Practical Guide*, edited by Z. Bai, J. Demmel, J. Dongarra, A. Ruhe, and H. Van der Vorst (SIAM, Philadelphia, 2000).

[47] This equation again features the high-frequency dielectric constant κ_∞, since we did not take into account the (average) response of the ions in the self-energy problem (see Ref. 35). The contribution of the ions to the self-energy should indeed almost completely cancel with the contribution of the ions to the electron and hole screening, the exciton being a neutral excitation (see discussion in Sec. III D).

[48] At large enough t/R, the InAs layer will be almost completely relaxed everywhere except around the interfaces with GaAs; the average hydrostatic strain will therefore decrease as the inverse of t.

[49] G. L. Bir and G. E. Pikus, *Symmetry and Strain-Induced Effects in Semiconductors* (Wiley, New York, 1974).

[50] G. Bastard, *Wave Mechanics Applied to Semiconductor Heterostructures* (Les Editions de Physique, Les Ulis, 1988).

[51] The wire has only a threefold symmetry axis along z (no cylindrical symmetry) due to the underlying atomic structure. There is no mirror plane perpendicular to y. This asymmetry is most clearly visible on the hole wave function at $t=16$ nm (see Fig. 8), though it also exists on Figs. 2, 3, and 5–7.

[52] This definition of the oscillator strength, meant to compare the different nanowires, does not include a $2/(1+\kappa_\infty)$ factor in F_x and F_y that would account for the ratio of the perpendicular field inside to the perpendicular field outside a nanowire [see, e.g., M. Califano and A. Zunger, Phys. Rev. B **70**, 165317 (2004)].

[53] M. Graf and P. Vogl, Phys. Rev. B **51**, 4940 (1995).

[54] S. Salon and M. V. K. Chari, *Numerical Methods in Electromagnetism* (Academic Press, San Diego, 1999).

[55] E. A. Muljarov, E. A. Zhukov, V. S. Dneprovskii, and Y. Masumoto, Phys. Rev. B **62**, 7420 (2000).

[56] R. Barrett, M. Berry, T. F. Chan, J. Demmel, J. Donato, J. Dongarra, V. Eijkhout, R. Pozo, C. Romine, and H. Van der Vorst, *Templates for the Solution of Linear Systems: Building Blocks for Iterative Methods*, 2nd ed. (SIAM, Philadelphia, 1994).